Modeling and Preview H_∞ Control Design for Motion Control of Elastic-Joint Robots With Uncertainties

Maria Makarov, Mathieu Grossard, Pedro Rodríguez-Ayerbe, *Member, IEEE*, and Didier Dumur

***Abstract*—This paper describes a novel approach combining identification and control design for motion control of multiple-link elastic-joint robots with motor sensors only and in presence of model uncertainties. The proposed model-based control design method makes use of the H_∞ (H-infinity) framework to design a two-degree-of-freedom controller with anticipation able both to 1) withstand uncertainties or variations in model parameters and 2) follow reference trajectories with prescribed precision thanks to a preview feedforward action which anticipates the future trajectory on a given time horizon. The proposed design methodology is experimentally evaluated on a two-degree-of-freedom lightweight robotic arm, which is first modeled and identified in the frequency domain. Experimental validation of the controller confirms that the objectives of the dynamic precision in trajectory tracking and tip vibration damping are both achieved. Additional analysis and numerical simulations illustrate how the presented preview H_∞ controller may be seen as an extension, with supplementary design parameters, of the traditional motor feedback with compensations based on the robot inverse dynamic model. A performance comparison between the proposed control method and the traditional inversion-based control shows the benefits of the anticipatory action and the possibilities offered by an H_∞ design framework for the management of tradeoffs in the specifications.**

***Index Terms*—Elastic-joint robots, frequency-domain identification, H-infinity control design, model uncertainties.**

I. Introduction

A. Problem Statement

THIS paper deals with serial robot manipulators with flexible transmission elements modeled by elastic joints. As the level of elasticities in robotic manipulators varies with the target applications and the mechanical design, different control solutions can be envisaged. On the one hand, traditional manufacturing robots developed for high precision may often be considered as essentially rigid, and position sensors at the motor level are sufficient in most applications. On the other hand, lightweight manipulators built to fit into a human environment with sufficient safety guarantees are more likely to display an intrinsic elastic behavior and are, therefore, equipped with suitable, often joint-level, additional position or torque sensors for precise control [1].

Between these two extremes, this study focuses on robots with moderate levels of joint elasticities due, for instance, to flexible transmissions, which cannot be neglected in the context of precise motion control, but which may not justify an integration of additional joint-level sensors. Such manipulators, with motor position sensors only, include both industrial robots lifting heavy payloads with respect to their proper mass, robotic structures of reduced cost which rigidity is not a primary goal, or even fully equipped robots exposed to sensor faults. The control objective is then to achieve the best performance in terms of trajectory tracking and vibration damping, which is possible using motor-side measurements only. To compensate the absence of joint-level sensors, model-based control design allows us to find powerful solutions, provided that the model uncertainties or parameter variations are taken into account in the design procedure.

To deal with the absence of joint sensors, several control strategies have been described in the literature. Model-based observers can be used to reconstruct missing measurements [2], [3]. As an alternative, a classical control scheme implements motor-level feedback control [for instance, proportional derivative (PD)] completed by direct compensations based on the robot inverse dynamic model [4]: for regulation tasks, gravity compensation is shown to be sufficient, while in trajectory tracking, a two-degree-of-freedom (dof) controller is used, where the feedback controller is completed with a feedforward compensation of the nominal reference trajectory torque. In the remaining paper, this controller is referred to as the inversion-based controller.

B. Contribution

In this paper, a novel approach combining identification and anticipatory two-dof controller design is proposed for motion control of multiple-link elastic-joint robots in presence of model uncertainties and when only motor sensors are available.

This extends the classical inversion-based controller in several ways.

1) Both the feedback and the preview feedforward controllers are designed using the H_∞ framework, which allows us to precisely take into account the competing

Manuscript received October 7, 2015; revised March 4, 2016; accepted April 23, 2016. Date of publication June 21, 2016; date of current version September 9, 2016.

M. Makarov, P. Rodríguez-Ayerbe, and D. Dumur are with the Laboratoire des Signaux et Systèmes, CentraleSupélec, CNRS, Université Paris-Sud, F91192 Gif-sur-Yvette, France (e-mail: maria.makarov@centralesupelec.fr; pedro.rodriguez@centralesupelec.fr; didier.dumur@centralesupelec.fr).

M. Grossard is with the Interactive Robotics Laboratory, CEA LIST, F-91190 Gif-sur-Yvette, France (e-mail: mathieu.grossard@cea.fr).

Color versions of one or more of the figures in this paper are available online at http://ieeexplore.ieee.org.

Digital Object Identifier 10.1109/TIE.2016.2583406

control objectives of robust stability, disturbance rejection, vibration damping, and dynamic precision.
2) The resulting feedforward control does not consist of a direct inversion of the robot dynamic model, but is designed on the already closed-loop system, thus increasing the overall robustness to model parameter variations.
3) The preview feedforward control is designed to anticipate the future trajectory on a specified time horizon for an improved tracking precision, whereas the classical inversion-based controller implements an intrinsic anticipation only through the acceleration terms.

In the following paragraphs, a brief literature review is provided about the model-based compensation in robotics, the robust control of robot manipulators including the use of H_∞ methods in control of elastic-joint robots under uncertainties, the control methods that include an anticipatory action over the future reference, and the identification of elastic-joint robots with motor sensors only.

C. Related Work

1) Model-Based Compensation: Thanks to the structure of their mathematical models, rigid (respectively, elastic-joint) manipulators can be linearized and decoupled by feedback, this property being related to the more general case of control of differentially flat systems. After such transformation, linear time-invariant (LTI) diagonal systems of double (respectively, quadruple) integrators are obtained [4]. Rigid model parameters are nowadays easily accessible from CAD tools and can also be obtained experimentally using well-established identification techniques [5]. In the elastic-joint case, a complete feedback linearizing control is impossible without additional sensors (joint position or torque), while the rigid case requires only motor-side sensors.

2) Robust Control: As the quality of the previously mentioned compensation heavily relies on the quality of the model, the benefits of robust design methods have been underlined very early in the rigid case [6] in association with various forms of inverse dynamic compensation (feedback linearizing control or feedforward compensations). The robustness problem with respect to uncertainties due to an imperfect feedback linearization was treated in [7] using μ-synthesis for a robot containing one elastic joint.

The H_∞ design was also used to reject the disturbances due to transmission nonlinearities [8], or to deal with the specification tradeoffs for a single-link robot under feedforward compensations [9]. While linear parameter-varying models have been considered in robust polytopic approaches [10], the direct exploitation of the experimental identification results for uncertainty characterization of elastic-joint arms as in [11] is not very common in robotics. Frequency-domain descriptions of uncertainty bounds for control are more frequently treated in the identification-for-control literature [12].

3) Anticipation: Beyond well-established two-dof controller structures with feedback and feedforward actions, the anticipation of the trajectory over a finite horizon is a convenient way to increase the tracking precision. Besides model-predictive control [13]–[15], two-dof controllers with anticipation (referred to as preview control in the dedicated literature [16]) can be designed using LQG, H_2 or H_∞ frameworks [17]–[21]. In the preview problem, the anticipatory effect is usually materialized by a delay between the anticipated reference and the controlled system inputs. The control design problem is then solved on the initial system, augmented with the delay dynamics. Recently, preview H_∞ control techniques have been applied for disturbance rejection within the robotic context in beating heart surgery [22] or in power grids [23]. Here, we consider an anticipatory feedforward action on the reference signal for trajectory tracking.

4) Identification: Within this study, the purpose of the experimental identification is to provide suitable models for the H_∞ control design. To reduce the complexity (order and structure) of the H_∞ controllers, a linearizing feedback based on the rigid model is first applied to partially compensate the robot dynamics. The resulting system, which would consist of a set of decoupled double integrators in a perfectly rigid case, but contains here elastic modes, is experimentally characterized in frequency domain. The pursued objective, therefore, differs from the one of the classical physical model parameter identification. Physical parameters of the complete elastic-joint robot model can be identified using additional measurements from joint position sensors, motion capture, accelerometers, or joint torque sensors, as, for instance, reported in [24]–[27]. Without additional sensors, existing dynamic identification methods for industrial robots with flexibilities are mainly based on simplified physical models combined with specifically designed closed-loop experiments in accordance with the assumed simplifications. Identification is then performed locally (single-joint approaches as in [25] and [28]), or globally through optimization over several identified local models [29].

In the objective of identifying a model for the H_∞ robust design, the selected approach is inspired by the methodology described in [29]. In the considered case of robots with motor-side measurements only and a moderate level of joint flexibilities, it is of interest of investigating to which point the control methods usually used for rigid robots apply, and when the control methods specifically designed for elastic-joint robots need to be implemented. In this paper, we investigated the effects of a rigid model-based compensation through the analysis of the resulting system model (5). We show that the identification can be used to bound the flexibilities effects in the model, in order to ensure a robust controller design regarding these uncertainties.

D. Outline

Section II introduces the modeling of elastic-joint robots with a rigid model-based linearizing feedback, which partially compensates the robot dynamics. Frequency-domain identification of the resulting system is described in Section III, and the experimental example of a two-link lightweight robotic arm is considered. The preview H_∞ control design for the previously identified system is detailed in Section IV, and experimental evaluation results are provided. Finally, in Section V, the proposed control method is compared with a classical inversion-based

control through numerical simulations, which allow us to consider multiple sets of values for the uncertain parameters.

II. Dynamic Modeling and Control-Oriented Analysis in Presence of Motor Sensors Only

In the perspective of a robust control design using motor measurements only, the dynamic models of rigid and elastic-joint robots are first briefly recalled. The effects of a rigid model-based feedback are examined, and a linear model for identification and control is obtained.

A. Dynamic Models of Robot Manipulators

Consider an n-link elastic-joint manipulator, in which the elastic effects of the motor-to-joint transmission are modeled by torsional springs of stiffness $\boldsymbol{K}$. Let $\boldsymbol{\theta} \in \mathbb{R}^n$ denote the motor angles after the reduction stage, $\boldsymbol{q} \in \mathbb{R}^n$ the joint angles, and $\boldsymbol{\tau} \in \mathbb{R}^n$ the motor torque after reduction. Assuming that the angular velocity of the rotors is due only to their own spinning, i.e., neglecting the inertial couplings between the motors and the links [4], the following reduced dynamic model of the elastic-joint robot can be obtained using the Lagrange formalism:

$$\boldsymbol{M_L}(\boldsymbol{q})\ddot{\boldsymbol{q}} + \boldsymbol{H}(\boldsymbol{q}, \dot{\boldsymbol{q}}) + \boldsymbol{\tau}_{fa} + \boldsymbol{K}(\boldsymbol{q} - \boldsymbol{\theta}) = 0 \tag{1}$$

$$\boldsymbol{J}\ddot{\boldsymbol{\theta}} + \boldsymbol{\tau}_{fm} + \boldsymbol{K}(\boldsymbol{\theta} - \boldsymbol{q}) = \boldsymbol{\tau} \tag{2}$$

with $\boldsymbol{M_L} \in \mathbb{R}^{n\times n}$ being the rigid body inertia matrix, $\boldsymbol{J} \in \mathbb{R}^{n\times n}$ the diagonal rotor inertia matrix, $\boldsymbol{K} \in \mathbb{R}^{n\times n}$ the diagonal matrix of joint stiffness, $\boldsymbol{\tau}_{fa}$ and $\boldsymbol{\tau}_{fm} \in \mathbb{R}^n$, respectively, the joint and motor friction torques, and $\boldsymbol{H} = \boldsymbol{C}(\boldsymbol{q}, \dot{\boldsymbol{q}})\dot{\boldsymbol{q}} + \boldsymbol{\tau}_G(\boldsymbol{q}) \in \mathbb{R}^n$ regrouping, respectively, the Coriolis and centrifugal torques $\boldsymbol{C}(\boldsymbol{q}, \dot{\boldsymbol{q}})\dot{\boldsymbol{q}}$ and the gravitational torques $\boldsymbol{\tau}_G(\boldsymbol{q})$.

In this framework, the purely rigid case corresponds to an infinite joint stiffness so that $\boldsymbol{\theta} = \boldsymbol{q}$, and the standard n-link rigid model can be written as follows:

$$\boldsymbol{M}(\boldsymbol{q})\ddot{\boldsymbol{q}} + \boldsymbol{H}(\boldsymbol{q}, \dot{\boldsymbol{q}}) + \boldsymbol{\tau}_f = \boldsymbol{\tau} \tag{3}$$

with $\boldsymbol{M} = \boldsymbol{M_L} + \boldsymbol{J}$ being the rotors and links inertia matrix and $\boldsymbol{\tau}_f$ the common friction torque.

B. Linearizing Control of Rigid Robots

Under the rigidity assumption, the robot's identification and control are fully accessible using only motor measurements. The model (3) being linear in the parameters, the latter can be identified using a weighted least-squares procedure. The conventional linearizing feedback control for the rigid motion is then

$$\boldsymbol{\tau} = \hat{\boldsymbol{M}}(\boldsymbol{q})\boldsymbol{u} + \hat{\boldsymbol{H}}(\boldsymbol{q}, \dot{\boldsymbol{q}}) \tag{4}$$

with the estimates $\hat{\boldsymbol{M}}(\boldsymbol{q})$ and $\hat{\boldsymbol{H}}(\boldsymbol{q}, \dot{\boldsymbol{q}})$ being updated at each sampling time, and the new control vector $\boldsymbol{u}$. In the case of perfectly known rigid dynamics (3), the control (4) leads to a linearized and decoupled system of input $\boldsymbol{u}$ and output $\boldsymbol{\theta}$, consisting of a set of n independent double integrators. An outer control loop can then be designed to control each axis as a linear single-input single-output (SISO) system.

C. Motor-Side-Based Modeling

The proposed approach, aimed at identifying and controlling the elastic-joint dynamics using motor sensors only, relies on the model (3) assumed known from preliminary experiments or CAD data, and the inner loop (4). The resulting system $\boldsymbol{\Sigma}$, of input $\boldsymbol{u}$ and output $\boldsymbol{\theta}$, does not consist n independent double integrators, as expected in the perfect rigid linearization case. It is instead still nonlinear, coupled, and affected by resonant elastic modes.

In the robust control design perspective, the system $\boldsymbol{\Sigma}$ is linearized around an equilibrium point $\dot{\boldsymbol{\theta}}_0 = 0$, $\dot{\boldsymbol{q}}_0 = 0$, $\boldsymbol{\theta}_0 = \boldsymbol{q}_0 + \boldsymbol{K}^{-1}\boldsymbol{\tau}_{G_0}$, with $\boldsymbol{\tau}_{G_0} = \boldsymbol{\tau}_G(q_0)$ being the gravity torque at $\boldsymbol{q}_0$. The friction terms $\boldsymbol{\tau}_{fa} = \boldsymbol{F}_v\dot{\boldsymbol{q}}$ and $\boldsymbol{\tau}_{fm} = \boldsymbol{F}_{vm}\dot{\boldsymbol{\theta}}$ are assumed to represent the viscous friction contribution with coefficients $\boldsymbol{F}_v$ and $\boldsymbol{F}_{vm}$.

The system $\boldsymbol{\Sigma}$ can then locally be written as an LTI system in the Laplace domain, with s being the Laplace variable:

$$\boldsymbol{\Theta}(s) = \boldsymbol{G}(s)\boldsymbol{U}(s). \tag{5}$$

The term $G_{ij}(s)$ of the matrix $\boldsymbol{G}$ in (5) represents the influence of input u_j on output θ_i. For instance, in a two-dof arm case ($n = 2$), $G_{ij}(s)$ has the following form:

$$G_{ij}(s) = \frac{a_0(s + a_1)(s^2 + a_2 s + a_3)(s^2 + a_4 s + a_5)}{s(s + b_1)(s + b_2)(s^2 + b_3 s + b_4)(s^2 + b_5 s + b_6)} \tag{6}$$

where a_i and b_j are real scalar coefficients that depend on the robot dynamic parameters, among which the stiffness and friction parameters. Particularly, such a gray-box approach allows us to consider parametric uncertainties.

III. Frequency-Domain Identification

In this section, a gray-box identification in frequency domain is applied to an elastic-joint robot manipulator (1), (2) under the rigid model-based feedback (3) in order to validate the proposed control-oriented model (6) and to estimate its unknown elastic parameters F_{v_i}, F_{vm_i}, K_i. The rigid model is assumed to be known from previous identification experiments and CAD data. In a two-step procedure inspired by [29], the frequency response function (FRF) of the system of interest is first estimated, and the model parameters are then obtained by optimization with regard to the parametric theoretical frequency response of the system (6). For the experimental evaluation, the ASSIST robot arm (see Fig. 1) is considered.

A. Nonparametric Frequency Response Estimation

A frequency-domain approach is well suited for the modeling and control of elastic-joint robots as the elastic modes can be easily observed and validated. Moreover, it provides a way to extract frequency-domain information about the model uncertainties which may be used for the robust control design.

1) Input Design: The choice of odd random phase multisines is suggested in [30] to obtain the best linear approximation of a dominantly linear system under nonlinear distortions. Besides the properties of multisines for frequency-domain

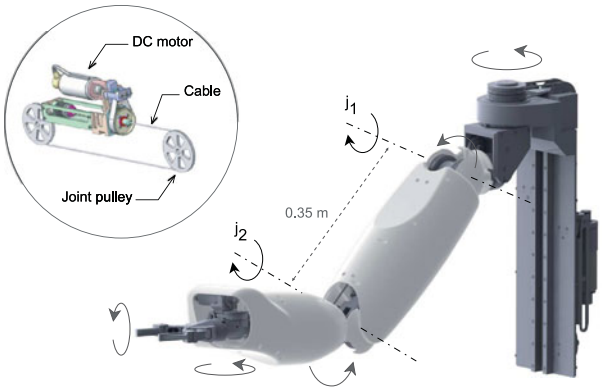

Fig. 1. ASSIST robot arm with two actuated joints $\{j_1, j_2\}$ considered in this study and five other dofs, with an illustration of the actuation principle.

identification as periodic signals, the use of a random phase allows averaging the FRF over several realizations to reduce the nonlinear effects and, thus, combines the benefits of random and periodic excitation. A random phase multisine is defined as

$$u(t) = \sum_{k=1}^{N_f} A_k \cos(\omega_k t + \phi_k) \tag{7}$$

with $\omega_k \in \{\frac{2\pi l}{N_p T_s},\ l = 0, 1, \ldots, \frac{N_p}{2} - 1\}$. N_f is the number of excited frequencies ω_k, A_k the signal amplitudes, ϕ_k the random phases uniformly distributed on $[0, 2\pi]$, T_s the sampling time, and N_p (even integer) the length of the signal. Odd random phase multisines can be used to excite only the odd harmonics in order to minimize the influence of nonlinearities in the estimation [30]. A specific power spectrum $\Phi_u(\omega)$ is achieved using amplitudes

$$A_k = 2\sqrt{\Phi_u(\omega_k)/N_p}. \tag{8}$$

Consider a SISO system $y = Gu + v$, with v being the measurement noise, under feedback $u = -F_{\text{ident}} y + r$. Only the power spectrum Φ_r of the reference signal r can be explicitly defined in closed-loop experiments. However, the spectrum Φ_u of the system input u is of crucial importance for the quality of the experimental FRF estimation. In the elastic robot identification, a flat power spectrum Φ_r typically results in a low signal-to-noise ratio and, thus, a high variance at low and resonant frequencies. Therefore, Φ_r needs to be carefully designed to achieve a suitable input spectrum Φ_u. The input and the reference power spectra are connected by

$$\Phi_u = |S_G|^2 \Phi_r + |S_G|^2 |F_{\text{ident}}|^2 \Phi_v \tag{9}$$

where $S_G = (1 + F_{\text{ident}} G)^{-1}$ is the closed-loop sensitivity function and Φ_v is the noise spectrum. Therefore, if the controller F_{ident} and the system G are known, to achieve an input spectrum close to a given spectrum Φ_u, the following reference spectrum can be considered:

$$\Phi_r = \frac{1}{|S_G|^2} \Phi_u. \tag{10}$$

In an identification procedure aimed at identifying G, prior knowledge can be used to design the spectrum. An approximation G_{ident} of G can be estimated from the physical principles or from an initial identification experiment to be refined.

2) Multivariable Frequency Response Estimation:

Consider a linear system $\boldsymbol{G}$ with n_u inputs $\boldsymbol{u}$ and n_y outputs $\boldsymbol{y}$. Assuming periodic data affected by measurement noise $\boldsymbol{V}$, with $\boldsymbol{U}(\omega_k)$ and $\boldsymbol{Y}(\omega_k)$ being the discrete Fourier transforms (DFT) of the input $\boldsymbol{u}$ and output $\boldsymbol{y}$ at frequency ω_k, the following input–output relation holds:

$$\boldsymbol{Y}(\omega_k) = \boldsymbol{G}(\omega_k)\boldsymbol{U}(\omega_k) + \boldsymbol{V}(\omega_k). \tag{11}$$

To estimate $\boldsymbol{G}(\omega_k) \in \mathbb{C}^{n_y \times n_u}$, data from $n_e \geq n_u$ different experiments are collected

$$\underline{\boldsymbol{Y}}(\omega_k) = \boldsymbol{G}(\omega_k)\underline{\boldsymbol{U}}(\omega_k) + \underline{\boldsymbol{V}}(\omega_k) \tag{12}$$

where $\underline{\boldsymbol{U}}(\omega_k) \in \mathbb{C}^{n_u \times n_e}$ and $\underline{\boldsymbol{Y}}(\omega_k) \in \mathbb{C}^{n_y \times n_e}$.

Different estimators can be used to compute the FRF $\hat{\boldsymbol{G}}$ from (12). In this study, an arithmetic mean is used to average the FRF over the experiments

$$\hat{\boldsymbol{G}}(\omega_k) = \frac{1}{N_e} \sum_{m=1}^{N_e} \left[\hat{\boldsymbol{G}}^{[m]}\right], \hat{\boldsymbol{G}}^{[m]} = \underline{\boldsymbol{Y}}^{[m]}(\omega_k) \left[\underline{\boldsymbol{U}}^{[m]}(\omega_k)\right]^{-1} \tag{13}$$

assuming $n_y = n_u$ and $n_e = N_e \times n_u$ experiments in order to partition the system (12) into N_e integer number of blocks $\underline{\boldsymbol{Y}}^{[m]}(\omega_k)$ and $\underline{\boldsymbol{U}}^{[m]}(\omega_k)$ of size $n_u \times n_u$.

The sample variance of the arithmetic mean estimator is computed as follows:

$$\hat{\boldsymbol{\sigma}}_{\hat{G}}(\omega_k)^2 = \frac{1}{N_e(N_e - 1)} \sum_{m=1}^{N_e} \left|\hat{\boldsymbol{G}}^{[m]}(\omega_k) - \hat{\boldsymbol{G}}(\omega_k)\right|^2. \tag{14}$$

B. Flexible Parameter Estimation

In the second step of the identification procedure, the discretized parametric model (6) of the elastic-joint robot is fitted to the nonparametric FRF. The rigid parameters are fixed to the previously identified values and used in the rigid model-based inner loop. The elastic parameters to be identified are the joint stiffness matrix $\boldsymbol{K} \in \mathbb{R}^{n \times n}$ and the joint and the motor viscous friction coefficients $\boldsymbol{F}_v$ and $\boldsymbol{F}_{vm}$. For an improved numerical stability and robustness to outliers, the parameter vector $\boldsymbol{p}_{\text{flex}}$ is estimated in a weighted logarithmic least-squares procedure over the frequency response magnitudes

$$\boldsymbol{p}_{\text{flex}}^{\text{opt}} = \arg\min_{\boldsymbol{p}_{\text{flex}}} \boldsymbol{V}_{\text{cost}}(\boldsymbol{p}_{\text{flex}}) \tag{15}$$

$$\boldsymbol{V}_{\text{cost}} = \sum_{k=1}^{N_p} \left|\log\left(|\boldsymbol{G}(\omega_k)|\right) - \log\left(\left|\hat{\boldsymbol{G}}(\omega_k)\right|\right)\right|^2 \boldsymbol{W}_k. \tag{16}$$

The weighting matrices $\boldsymbol{W}_k = \boldsymbol{W}(\omega_k)$ can be defined to emphasize the optimization on a particular frequency interval. In this study, the inverse of the sample standard deviation $\boldsymbol{W}_k = \left(\hat{\boldsymbol{\sigma}}_{\hat{G}}(\omega_k)\right)^{-1}$ is used.

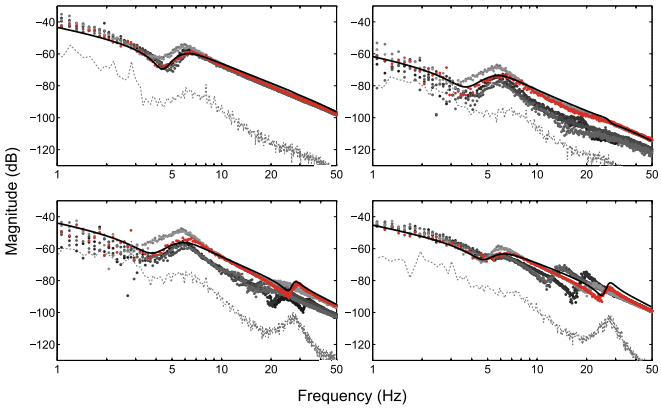

Fig. 2. Experimental nonparametric MIMO FRF $\hat{\boldsymbol{G}}$ in the tested configurations (dots), sample standard deviation of the nonparametric estimate $\hat{\boldsymbol{\sigma}}_{\hat{G}_0}$ in nominal configuration (dashed gray), and theoretical nominal parametric $\boldsymbol{G}_0$ (solid line) MIMO FRF.

C. Experimental FRF of the ASSIST Robot Arm

In this section, the previously described modeling and identification procedure is applied on the lightweight and elastic-joint ASSIST robot arm, whose rigid parameters are identified in [31] using a conventional rigid identification method based on linear least squares.

1) System Under Consideration: Without loss of generality, the seven-dof ASSIST robot arm is considered here as a two-joint manipulator, where the shoulder j_1 and the elbow j_2 only are actuated, the other five rotational dof being fixed (see Fig. 1). The robot motion is thus restricted to the vertical plane. With the compensation (3), this system corresponds to the theoretical model (6). In a mechanical design focused on a safe human–robot interaction, the joint actuators are based on a screw-and-cable mechanism achieving a high mechanical backdrivability [31]. DC motors driven by pulse-width-modulated servo amplifiers in torque mode are employed. The motor shafts are equipped with incremental position encoders. The robot arm is controlled by a real-time dedicated controller running VxWorks, with a sampling time $T_s = 4$ ms.

2) Experiment Design and Results: As the local model (5) depends on the robot configuration $\boldsymbol{q}_0$, the identification experiments are performed in $n_{\text{config}} = 7$ configurations selected as extremal with respect to the joint position ranges, corresponding for each of the two joints to $q_i^{\min} = -\pi/2$ rad, $q_i^{\text{med}} = 0$ rad, and $q_i^{\max} = \pi/2$ rad. Random phase multisines are used as input signals for the closed-loop identification, with odd frequencies selected over the range 0.5–50 Hz. Each joint is excited separately, with six realizations of the input signal, resulting in $n_e = 6 \times 2$ experiments. The used signal length is $N_p = 2^{12}$ points. The input spectrum design method (10) is applied to the different axes of the robot using $G_{\text{ident}}(s) = \omega_r^2/\omega_a^2 \cdot (s^2 + 2\xi\omega_a s + \omega_a^2)/(s^2(s^2 + 2\xi\omega_r s + \omega_r^2))$ obtained from preliminary identification results, and a PD controller $F_{\text{ident}}(s) = K_p + K_d s$.

Fig. 2 shows the frequency responses $\hat{\boldsymbol{G}}$ of the two-dof ASSIST arm in the tested configurations, which are in accordance with the theory: two elastic modes corresponding to the two elastic joints are observed. As expected in the case of collocated pairs of motors and motor sensors, each antiresonance in the diagonal terms is followed by a resonance. The first resonance is centered around 6 Hz with ca. 1-Hz dispersion due to the configuration variations. The second resonance, mainly visible in the j_2 responses, varies between 13 and 30 Hz. Fig. 2 also illustrates the correspondence between the experimental nonparametric FRF estimate $\hat{\boldsymbol{G}}_0$ given with its sample standard deviation $\hat{\boldsymbol{\sigma}}_{\hat{G}}$, and the fitted parametric model $\boldsymbol{G}_0$ in the nominal configuration. The obtained elastic parameters for this configuration are $\boldsymbol{K} = \text{diag}\{699.7,\ 645.0\}\,\text{N·m·rad}^{-1}$, $\boldsymbol{F}_v = \text{diag}\{1.79,\ 0.42\}\,\text{N·m·s·rad}^{-1}$, $\boldsymbol{F}_{vm} = \text{diag}\{41.44,\ 5.41\}\,\text{N·m·s·rad}^{-1}$. The difference in the motor viscous friction coefficients $\boldsymbol{F}_{vm}$ may be explained by the presence of additional reduction gears on the first motor.

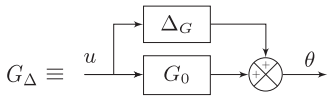

Fig. 3. Uncertain model $\boldsymbol{G}_\Delta$ with additive uncertainty $\boldsymbol{\Delta}_G$ and nominal model $\boldsymbol{G}_0$.

D. Uncertainty Description

The system $\boldsymbol{\Sigma}$ resulting from the control (4) applied to (1) and (2) is seen in the following as uncertain. The nominal model denoted $\boldsymbol{G}_0$ corresponds to the identified model in the extended horizontal position of the arm ($q_1 = 0$ rad, $q_2 = 0$ rad). An additive unstructured uncertainty $\boldsymbol{\Delta}_G$, to be taken into account in the control design for robust closed-loop stability, represents the variations of the system around this nominal configuration, as well as variations of the system's parameters which may be due to wear, temperature-dependent friction, or a payload (see Fig. 3).

For robust control design, the estimated upper bound of $\boldsymbol{\Delta}_G$ is approximated in frequency domain by $W_\Delta(s)$. In the case where it models the variations of the system around the nominal configuration, the uncertainty $\boldsymbol{\Delta}_G$ can be characterized from the previous identification experiments by $\boldsymbol{\Delta}_G(\omega_k) = \max_i |\boldsymbol{G}_0(\omega_k) - \hat{\boldsymbol{G}}_i(\omega_k)|$, where $\boldsymbol{G}_0$ is the nominal model and $\hat{\boldsymbol{G}}_i$ the estimated frequency response in the ith configuration ($i = 1 \ldots n_{\text{config}}$). As said before, in addition to this definition, $\boldsymbol{\Delta}_G$ can include model variations due to uncertain parameters.

IV. H_∞ Preview Control Design

This section presents the design of an anticipative two-dof controller satisfying the objectives of robustness, damped disturbance rejection, and trajectory tracking, using motor-side information only for the previously identified system. Following the frequency-domain approach in continuity with the identification procedure, the specifications for this controller are expressed by frequency weighting functions, and the design of the preview two-dof controller is performed using H_∞ techniques.

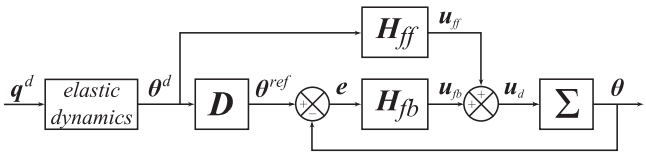

Fig. 4. Preview H_∞ control method.

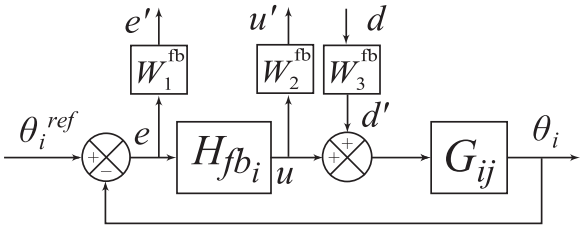

Fig. 5. Feedback controller design.

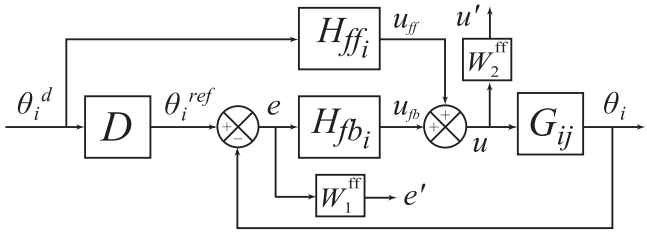

Fig. 6. Feedforward controller design.

TABLE I
DISCRETIZED H_∞ (H_{FB}) CONTROLLERS EVALUATED ON THE NOMINAL MODEL

H_{fb}	M_φ (°)	ω_c (Hz)	M_G (dB)	M_τ	$\lvert S_y\rvert_{dB}^{max}$	$\lvert T_y\rvert_{dB}^{max}$
Joint 1	71.3	26.7	8.37	1.9	4.89	0
Joint 2	65.9	31.7	9.09	1.5	4.96	0.20

ω_c is the open-loop crossover frequency, M_G (M_φ) is the gain (phase) margin, and M_τ is the delay margin in samples.

A. Preview H_∞ Control Design Methodology

Fig. 4 depicts the two-dof controller structure with a feedforward action for reference preview intended to improve the tracking accuracy. Information about future reference is provided to the controller with an anticipation horizon t_a, materialized at the controller's input by a delay D between the anticipated reference and the system input.

The control problem is thus solved for the initial system augmented with the delay. In this study, the feedforward and feedback components H_{ff} and H_{fb} of the controller are designed in a two-step sequential procedure for each joint. SISO continuous-time approximate models $\tilde{G}_{0_{1,2}}(s)$ of $\boldsymbol{G}_0$ are used to limit the order of the controllers. The controllers obtained from H_∞ synthesis are reduced by the balanced realization method, an integral action is isolated in H_{fb} to ensure zero static error, and the resulting controllers are discretized using the bilinear transform for real-time implementation.

1) Feedback Controller Design: In a first step, H_{fb} is designed for each joint using the augmented system in Fig. 5. Here, $\tilde{G}_0(s)$ denotes $\tilde{G}_{0_{1,2}}(s)$, respectively, for joint 1 or 2. In a classical four-block H_∞ control scheme, the closed-loop transfers (17) are shaped by weightings W_1^{fb}, W_2^{fb}, W_3^{fb}:

$$\begin{pmatrix} e' \\ u' \end{pmatrix} = \begin{pmatrix} W_1^{\text{fb}} S_y & -W_1^{\text{fb}} S_y \tilde{G}_0 W_3^{\text{fb}} \\ W_2^{\text{fb}} H_{\text{fb}} S_y & -W_2^{\text{fb}} T_u W_3^{\text{fb}} \end{pmatrix} \begin{pmatrix} \theta_i^{ref} \\ d \end{pmatrix} \tag{17}$$

with the direct and complementary sensitivity functions

$$S_y(s) = \left(1 + \tilde{G}_0(s) H_{\text{fb}}(s)\right)^{-1} \tag{18}$$

$$T_u(s) = \left(1 + H_{\text{fb}}(s) \tilde{G}_0(s)\right)^{-1} H_{\text{fb}}(s) \tilde{G}_0(s). \tag{19}$$

The H_∞ control problem is then formulated as follows:

$$\min \gamma \tag{20}$$

$$\text{s.t.} \left\| \begin{matrix} W_1^{\text{fb}} S_y & -W_1^{\text{fb}} S_y \tilde{G}_0 W_3^{\text{fb}} \\ W_2^{\text{fb}} H_{\text{fb}} S_y & -W_2^{\text{fb}} T_u W_3^{\text{fb}} \end{matrix} \right\|_\infty < \gamma. \tag{21}$$

The general expression of the weightings used is provided by

$$W_1^{\text{fb}} = k_1^{\text{fb}} W_{\text{notch}},\ W_2^{\text{fb}} = k_2^{\text{fb}} W_\Delta \tag{22}$$

$$W_3^{\text{fb}} = \frac{1}{W_{13}^{\text{fb}} W_1^{\text{fb}}},\ \frac{1}{W_{13}^{\text{fb}}} = k_{13} \frac{Ks + \omega_{c13}\varepsilon}{s + \omega_{c13}} \tag{23}$$

with

$$W_{\text{notch}} = \frac{s^2 + \alpha s + \omega_0^{\min}\omega_0^{\max}}{s^2 + \epsilon_{\max}\alpha s + \omega_0^{\min}\omega_0^{\max}} \tag{24}$$

$$\alpha = \frac{\omega_0^{\max} - \omega_0^{\min}}{\bar{\epsilon}} \sqrt{\frac{1 - \bar{\epsilon}^2}{1 - \epsilon_{\max}^2}},\ \epsilon_{\max} < \bar{\epsilon}. \tag{25}$$

2) Feedforward Controller Design: In the second step, the preview feedforward controller is designed to minimize the tracking error. The augmented system in Fig. 6 is composed of the previously designed closed loop with H_{fb} before reduction, the bloc $D(s)$ equivalent to a time delay of N_a samples, obtained from $D(z) = z^{-N_a}$ by the inverse bilinear transform, and weightings W_1^{ff} and W_2^{ff} given by (26) and (27). The main design objective of this step is to shape S_y by W_1^{ff} to obtain the desired dynamic accuracy. Additionally, W_2^{ff} is used to limit the control effort:

$$W_1^{\text{ff}} = k_1^{\text{ff}} W_{\text{notch}} W_{10} \tag{26}$$

$$W_2^{\text{ff}} = k_2^{\text{ff}} W_\Delta,\ \frac{1}{W_{10}} = \left(\frac{\sqrt{K}s + \omega_{c1}\sqrt{\varepsilon}}{s + \omega_{c1}}\right)^2. \tag{27}$$

B. Experimental Evaluation

1) Design Results: For each joint, an H_{fb} controller of order 12 is obtained with the MATLAB *Robust Control Toolbox* and is reduced to order 8. After discretization, γ equals 2.25 for j_1 and 2.79 for j_2. The stability margins are provided in Table I for the SISO designs of both joints.

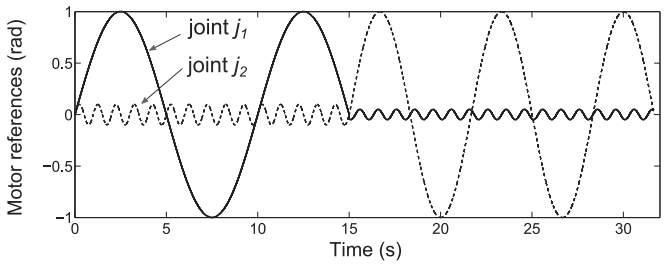

Fig. 7. Motor references in experiment 1 (j_1 solid, j_2 dashed).

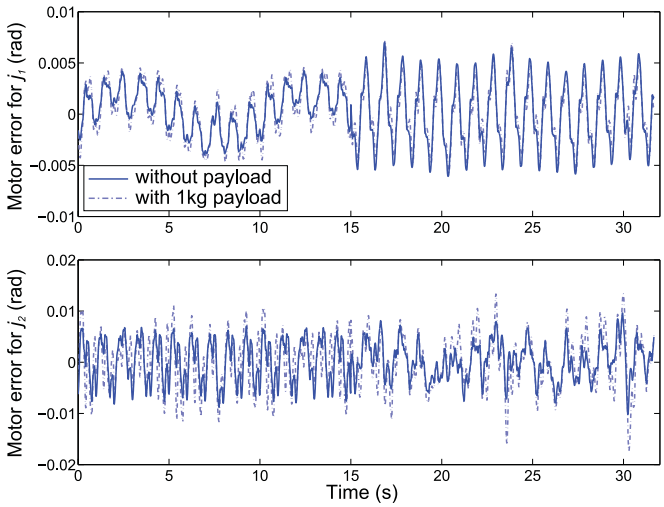

Fig. 8. [Experimental] Motor tracking error in experiment 1 with two-dof H_∞ controller without payload (solid) and with 1-kg payload (dashed).

In a tradeoff between the obtained performance and the order of H_{ff}, an horizon $N_a = 7$ is selected. A controller H_{ff} of order 30 is thus obtained for each joint and then reduced to order 12 and discretized.

2) Experimental Evaluation: The previously designed controller is evaluated on the ASSIST robot arm. Trajectory tracking at the motor level and step disturbance rejection at the end-effector are compared in the nominal conditions and with an unmodeled 1-kg payload attached to the arm.

In experiment 1, joints j_1 and j_2 are simultaneously actuated along sinusoidal motor references (see Fig. 7). High-amplitude and low-frequency references are used to evaluate the controller robustness to varying configurations (an amplitude of 1 rad for j_1 leads to a vertical displacement of 1.35 m). Low-amplitude and higher frequency references are used to evaluate the controller performance under disturbances due to the dynamic couplings between the joints.

Fig. 8 shows the motor tracking error in experiment 1 with and without 1-kg payload. The tracking error on j_2 is slightly higher than on j_1 due to the couplings. The impact of the payload is very limited thanks to the robustness properties of the preview H_∞ controller.

In experiment 2, the reference robot arm position is the extended horizontal configuration ($q_1 = 0,\ q_2 = 0$), and an additional load of 1 kg is attached to its end. The load is suddenly suppressed to create a joint torque step disturbance. A Leica laser tracker *LTD800* measures the 3-D position of a reflector fixed at the arm tip. The resulting vertical displacement is shown in Fig. 9. The vibrations due to the disturbance are effectively damped within 1 s by the controller, both in the nominal and the payload cases.

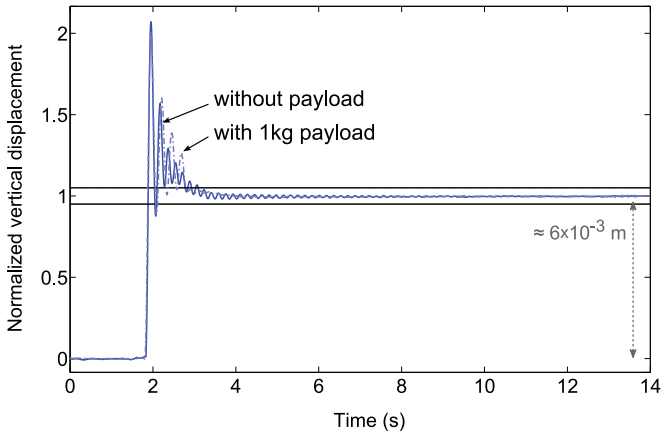

Fig. 9. [Experimental] Normalized vertical displacement of the robot's tip in experiment 2 with two-dof H_∞ controller without payload (solid) and with 1-kg payload (dashed). Horizontal lines mark 5% of final value.

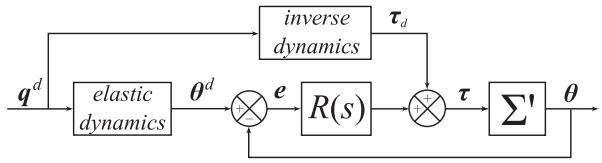

Fig. 10. Inversion-based control method.

V. Comparison of Elastic-Joint Robot Control Methods in Presence of Uncertainties

In this section, a comparison between the classical inversion-based control (see Fig. 10) and the proposed control (see Fig. 4) is conducted with respect to their robustness properties and performance in presence of modeling uncertainties. This comparison is illustrated by numerical simulation results.

A. Comparison Method

The classical inversion-based control (see Fig. 10) has a two-dof structure, where a PD feedback controller is completed with a feedforward compensation of the nominal reference trajectory torque. Here, an integral action is added to the traditional PD controller to allow fair comparisons with $H_{\text{fb}}(s)$. The resulting PID controller is denoted $\boldsymbol{R}(s)$ and its gains are selected so as to approach similar robust stability and bandwidth properties of the feedback controller H_{fb} presented in Table I.

The overall structure of both methods is similar (see Figs. 4 and 10). In both methods, knowing the desired link motion $\boldsymbol{q}^d$, the nominal motor trajectory $\boldsymbol{\theta}^d$ can be deduced from (1).

In the inversion-based control, the feedforward compensation consists in the nominal torque $\boldsymbol{\tau}^d$, computed as a function of $\boldsymbol{q}^d$ and its time derivatives up to the fourth order [4]. In the proposed method, the feedforward compensation is generated through H_{ff} with an anticipation over the future trajectory.

The goal of the present section is to analyze and compare the behavior of the two control structures in presence of uncertainties, both in frequency and time domains. In the numerical simulations, several randomly generated sets of the uncertain parameters values are used. Uncertain model parameters include the rigid body parameters (inertia, mass properties) and the flexible parameters (joint stiffnesses, motor and joint viscous friction coefficients). The rigid body (respectively, flexible) parameters are considered to be affected by $\pm 10\%$ (respectively, 30%) uncertainty. Indeed, the flexible parameters' identification is less accurate when compared to the rigid body properties which can also be known from CAO. In addition to that, the excursion of the mass parameters of the rigid links is augmented to model up to 3 kg of payload fixed at the end-effector of the robot. The lightweight ASSIST robot arm can lift important loads in comparison with its own weight, and the 3-kg payload, therefore, results in variations over 100% for the mass parameters of the links.

B. Frequency-Domain Comparison

In this section, using linear analysis, the expressions of the closed-loop sensitivity functions are derived for both methods in presence of model uncertainties. Let us first note that in Figs. 4 and 10, the nonlinear systems $\boldsymbol{\Sigma}$ and $\boldsymbol{\Sigma}'$ are not the same. $\boldsymbol{\Sigma}'$ represents the complete nonlinear elastic-joint arm, while $\boldsymbol{\Sigma}$ contains in addition the rigid model-based compensation. To use a common formalism for the comparison of this two control structures, linear analysis is first performed around an operating point to evaluate the sensitivity functions. The nonlinear system $\boldsymbol{\Sigma}$ (respectively, $\boldsymbol{\Sigma}'$) is represented in the Laplace domain by its transfer matrix $\boldsymbol{G}(s)$ (respectively, $\boldsymbol{G}'(s)$) and it nominal model used in the computations $\boldsymbol{G}_0(s)$ (respectively, $\boldsymbol{G}'_0(s)$). Within the inversion-based control scheme (see Fig. 10), the inverse dynamics compensation is conventionally denoted $\boldsymbol{\tau}^d = (\boldsymbol{G}'_0)^{-1}(s)\boldsymbol{\theta}^d$.

In presence of uncertainties (i.e., $\boldsymbol{G} \neq \boldsymbol{G}_0$ and $\boldsymbol{G}' \neq \boldsymbol{G}'_0$), the direct sensitivity functions, defined as transfers from $\boldsymbol{\theta}^d$ to $\boldsymbol{e}$, and denoted $\boldsymbol{S}_1(s)$ for the inversion-based control and $\boldsymbol{S}_2(s)$ for the preview H_∞ control, can be expressed as

$$\boldsymbol{S}_1(s) = (\boldsymbol{I}_n + \boldsymbol{G}'\boldsymbol{R})^{-1}(\boldsymbol{I}_n - \boldsymbol{G}'(\boldsymbol{G}'_0)^{-1}) \tag{28}$$

$$\boldsymbol{S}_2(s) = (\boldsymbol{I}_n + \boldsymbol{G}\boldsymbol{H}_{\text{fb}})^{-1}(\boldsymbol{D} - \boldsymbol{G}\boldsymbol{H}_{\text{ff}}). \tag{29}$$

It can be observed through the $\boldsymbol{S}_1(s)$ transfer matrix that if the system knowledge is perfect, a perfect tracking can be achieved by the inversion-based control. In the following, the case with uncertainty is considered. The complementary sensitivity functions (transfers from $\boldsymbol{\theta}^d$ to $\boldsymbol{\theta}$) denoted $\boldsymbol{T}_1(s)$ for the inversion-based control and $\boldsymbol{T}_2(s)$ for the preview H_∞ control can be expressed as

$$\boldsymbol{T}_1(s) = (\boldsymbol{I}_n + \boldsymbol{G}'\boldsymbol{R})^{-1}(\boldsymbol{G}'(\boldsymbol{G}'_0)^{-1} + \boldsymbol{G}'\boldsymbol{R}) \tag{30}$$

$$\boldsymbol{T}_2(s) = (\boldsymbol{I}_n + \boldsymbol{G}\boldsymbol{H}_{\text{fb}})^{-1}(\boldsymbol{G}\boldsymbol{H}_{\text{ff}} + \boldsymbol{G}\boldsymbol{H}_{\text{fb}}\boldsymbol{D}). \tag{31}$$

From the inspection of these expressions, the proposed method may be seen as an extension of the inversion-based control as it offers additional design dofs with the specifically designed feedforward controller including anticipation and a more general feedback controller. Table II presents the maximum H_∞ gain of the multivariable sensitivity and complementary sensitivity functions, evaluated for 100 sets of uncertain parameters on the linearized models. Smaller dispersion is observed in the preview H_∞ control case, and the peaks due to the resonances are better controlled through the explicit specifications of the weighting functions in the design step.

TABLE II
MAXIMUM H_∞ GAIN OF THE MULTIVARIABLE DIRECT SENSITIVITY S_y AND COMPLEMENTARY SENSITIVITY T_y FUNCTIONS

Controller	$\lvert\boldsymbol{S}\rvert^{\max}_{\text{dB}}$	$\lvert\boldsymbol{T}\rvert^{\max}_{\text{dB}}$
Inversion-based control with PID	12.35	20.08
Preview H_∞ control	7.02	8.46

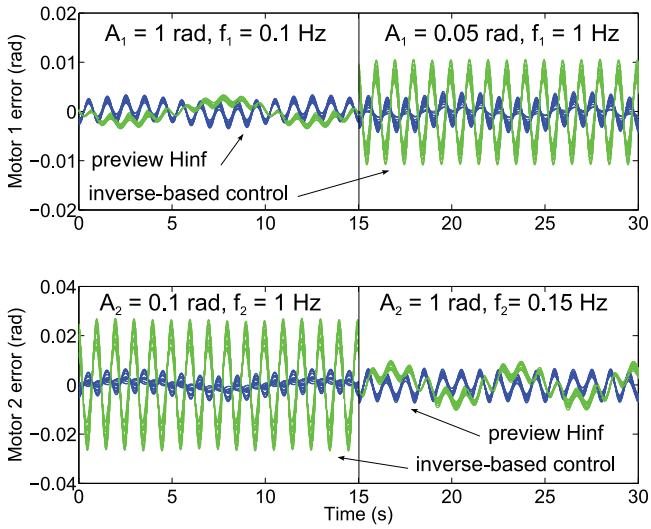

Fig. 11. [Simulation with uncertain parameters] Motor tracking errors in experiment 1 with preview H_∞ (blue) and inversion-based controller with PID (green).

C. Time-Domain Comparison

The complete nonlinear model of the robotic system is then used to simulate the time responses for 20 sets of uncertain parameters. Fig. 11 illustrates the motor tracking error in joints j_1 and j_2 obtained for experiment 1 (see Section IV-B2) with both controllers. For low-frequency reference, the error amplitudes are similar, but for high-frequency references, the dynamic precision of the preview H_∞ control yields better results with

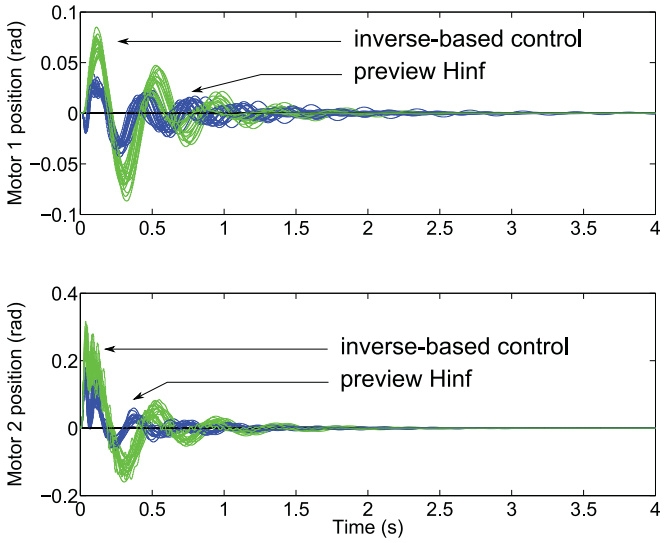

Fig. 12. [Simulation with uncertain parameters] Motor positions in the disturbance rejection experiment with preview H_∞ (blue) and inversion-based controller with PID (green).

respect to the maximum error amplitude and also the error amplitude dispersion for different uncertain parameters sets. Indeed, the dynamic precision as well as robustness can be taken into account in the control design through the choice of the weighting functions. Moreover, the preview H_∞ control benefits from a higher anticipation horizon N_a, which is another dof in the design.

Fig. 12 shows the motor positions in joints j_1 and j_2 in the disturbance rejection experiment with both controllers, in which an output step disturbance of 0.1 rad is applied to joint 2. A lower oscillation amplitude and faster damping is achieved with the preview H_∞ control, as well as a smaller dispersion for different parameters sets. The disturbance rejection properties are indeed also included in the weighting function selection when designing the H_∞ controller.

VI. Conclusion

In this paper, a global procedure was proposed for identification and robust control design for motion control of multiple-link elastic-joint robots using motor measurements only, in presence of uncertainties. A two-dof controller with anticipation was proposed and the H_∞ framework was used to solve the constrained control design problem with tradeoffs between specifications, such as the dynamic precision ensuring good trajectory tracking, damped disturbance rejection, and the robustness to uncertain or varying parameters.

The proposed identification and control design methodology especially applies to multijoint robots equipped with motor-side sensors only, in which the joint elasticities cannot be neglected to achieve accurate motion control. Due to its structure, the proposed controller can be applied without any restriction to manipulators with more than two dof.

The presented preview H_∞ controller may be seen an extension of the traditional motor feedback with compensations based on the robot inverse dynamic model. Since no compensations directly based on an inverse model are used, this controller demonstrates an increased robustness with respect to modeling uncertainties, which can arise from uncertain or varying parameters, as in the case of variable payload. In the same time, the tracking precision can be ensured thanks to the anticipatory feedforward action with a tunable time horizon.

References

[1] A. Albu-Schäffer, C. Ott, and G. Hirzinger, "A unified passivity-based control framework for position, torque and impedance control of flexible joint robots," *Int. J. Robot. Res.*, vol. 26, no. 1, pp. 23–39, Jan. 2007.

[2] M. Ruderman and M. Iwasaki, "Sensorless torsion control of elastic joint robots with hysteresis and friction," *IEEE Trans. Ind. Electron.*, Mar. 2015.

[3] B. Huard, M. Grossard, S. Moreau, and T. Poinot, "Sensorless force/position control of a single-acting actuator applied to compliant object interaction," *IEEE Trans. Ind. Electron.*, vol. 62, no. 6, pp. 3651–3661, Jun. 2015.

[4] A. De Luca andW. Book, "Robots with flexible elements," in *Springer Handbook of Robotics*, B. Siciliano and O. Khatib, Eds. Berlin, Germany: Springer, 2008, pp. 287–319.

[5] M. Gautier, "Dynamic identification of robots with power model," in *Proc. IEEE Int. Conf. Robot. Autom.*, Apr. 1997, vol. 3, pp. 1922–1927.

[6] W. Stout and M. Sawan, "Application of H_∞ theory to robot manipulator control," in *Proc. IEEE Conf. Control Appl.*, Sep. 1992, pp. 148–153.

[7] Z. Kang, T. Chai, K. Oshima, J. Yang, and S. Fujii, "Robust vibration control for SCARA-type robot manipulators," *Control Eng. Pract.*, vol. 5, no. 7, pp. 907–917, Jul.1997.

[8] M. Moghaddam and A. Goldenberg, "Nonlinear modeling and robust H_∞-based control of flexible joint robots with harmonic drives," in *Proc. IEEE Int. Conf. Robot. Autom.*, Apr. 1997, vol. 4, pp. 3130–3135.

[9] W.-S. Wang and C.-H. Liu, "Controller design and implementation for industrial robots with flexible joints," *IEEE Trans. Ind. Electron.*, vol. 39, no. 5, pp. 379–391, Oct. 1992.

[10] Z. Yu, H. Chen, and P.-y. Woo, "Gain scheduled LPV H_∞ control based on LMI approach for a robotic manipulator," *J. Robot. Syst.*, vol. 19, no. 12, pp. 585–593, Dec. 2002.

[11] S. Dadashi and H. Taghirad, "H-infinity controller design for a flexible joint robot with phase uncertainty," in *Proc. 39th Int. Symp. Robot.*, 2008, pp. 34–39.

[12] M. Gevers, "Identification for control: From the early achievements to the revival of experiment design," *Eur. J. Control*, vol. 11, no. 4, pp. 335–352, Jun. 2005.

[13] V. Upreti, S. Talole, and S. Phadke. (2004). "Predictive control of flexible joint robotic manipulator," in *Proc. Int. Conf. Cogn. Syst.*, [Online] Available: http://www.niitcrcs.com/iccs/iccs2004/

[14] R. Hedjar, R. Toumi, P. Boucher, and D. Dumur, "Finite horizon nonlinear predictive control by the taylor approximation: application to robot tracking trajectory," *Int. J. Appl. Math. Comput. Sci.*, vol. 15, no. 4, p. 527, Dec. 2005.

[15] M. Makarov, M. Grossard, P. Rodriguez-Ayerbe, and D. Dumur, "Comparison of two robust predictive control strategies for trajectory tracking of flexible-joint robots," in *Proc. IEEE/ASME Int. Conf. Adv. Intell. Mechatronics*, Jul. 2014, pp. 1704–1709.

[16] H. Peng and M. Tomizuka, "Preview control for vehicle lateral guidance in highway automation," *ASME J. Dyn. Syst., Meas., Control*, vol. 115, no. 4, pp. 679–686, Dec. 1993.

[17] K. Takaba, "A tutorial on preview control systems," in *Proc. SICE 2003 Annu. Conf.*, Aug. 2003, vol. 2, pp. 1388–1393.

[18] D. N. Hoover, R. Longchamp, and J. Rosenthal, "Two-degree-of-freedom $l2$-optimal tracking with preview," *Automatica*, vol. 40, no. 1, pp. 155–162, Jan. 2004.

[19] L. Mianzo and H. Peng, "Output feedback H_∞ preview control of an electromechanical valve actuator," *IEEE Trans. Control Syst. Technol.*, vol. 15, no. 3, pp. 428–437, May 2007.

[20] S. Ryu, Y. Kim, and Y. Park, "Robust h_∞ preview control of an active suspension system with norm-bounded uncertainties," *Int. J. Autom. Tech.*, vol. 9, no. 5, pp. 585–592, Oct. 2008.

[21] M. Kristalny and L. Mirkin, "Preview in h_2 optimal control: Experimental case studies," in *Proc. IEEE Conf. Decis. Control*, Dec. 2010, pp. 6004–6009.

[22] W. Bachta, P. Renaud, E. Laroche, A. Forgione, and J. Gangloff, "Active stabilization for robotized beating heart surgery," *IEEE Trans. Robot.*, vol. 27, no. 4, pp. 757–768, Aug. 2011.
[23] M. Babazadeh and H. Karimi, "A robust two-degree-of-freedom control strategy for an islanded microgrid," *IEEE Trans. Power Deliv.*, vol. 28, no. 3, pp. 1339–1347, Jul. 2013.
[24] A. Albu-Schaffer andG. Hirzinger, "Parameter identification and passivity based joint control for a 7 dof torque controlled light weight robot," in *Proc. IEEE Int. Conf. Robot. Autom.*, 2001, vol. 3, pp. 2852–2858.
[25] M. Pham, M. Gautier, and P. Poignet, "Identification of joint stiffness with bandpass filtering," in *Proc. IEEE Int. Conf. Robot. Autom.*, 2001, vol. 3, pp. 2867–2872.
[26] C. Lightcap and S. Banks, "Dynamic identification of a Mitsubishi PA10-6CE robot using motion capture," in *Proc. IEEE/RSJ Int. Conf. Intell. Robots Syst.*, Oct. 2007, pp. 3860–3865.
[27] J. Oaki and S. Adachi, "Grey-box modeling of elastic-joint robot with harmonic drive and timing belt," in *Proc. IFAC Symp. Syst. Identif.*, vol. 16, 2012, pp. 1401–1406.
[28] M. Östring, S. Gunnarsson, and M. Norrlöf, "Closed-loop identification of an industrial robot containing flexibilities," *Control Eng. Pract.*, vol. 11, no. 3, pp. 291–300, Mar. 2003.
[29] E. Wernholt and S. Moberg, "Nonlinear gray-box identification using local models applied to industrial robots," *Automatica*, vol. 47, no. 4, pp. 650–660, Apr. 2011.
[30] J. Schoukens, R. Pintelon, Y. Rolain, and T. Dobrowiecki, "Frequency response function measurements in the presence of nonlinear distortions," *Automatica*, vol. 37, no. 6, pp. 939–946, Jun. 2001.
[31] M. Makarov, M. Grossard, P. Rodriguez-Ayerbe, and D. Dumur, "Generalized predictive control of an anthropomorphic robot arm for trajectory tracking," in *Proc. IEEE/ASME Int. Conf. Adv. Intell. Mechatronics*, Jul. 2011, pp. 948–953.

Maria Makarov was born in Tomsk, Russia. She received the engineering degree in electrical Engineering from the École Supérieure d'Électricité (Supélec), Gif-sur-Yvette, France, the M.Sc. degree in electrical engineering from the KTH Royal Institute of Technology, Stockholm, Sweden, in 2010, and the Ph.D. degree in automatic control jointly from Supélec and the Université Paris-Sud, Orsay, France, in 2013.

Since 2013, she has been with the Automatic Control Department, CentraleSupélec, Gif-sur-Yvette, where she is currently an Assistant Professor. Her research interests include predictive and robust control for uncertain systems, with applications in robotic manipulation.

Mathieu Grossard was born in Besançon, France. He received the Engineering diploma and the M.Sc. degree in robotics and automation from the École Centrale de Nantes, Nantes, France, in 2005, and the Ph.D. degree in automatic control (best French Ph.D. award from the "GDR MACS") from FEMTO-ST, Besançon, in 2008.

Since 2008, he has been a Researcher with the Interactive Robotics Laboratory, CEA LIST, Gif-sur-Yvette, France, where he is involved in research on robotic manipulation and advanced control. In particular, his current research interests include optimal design, modeling, and robust control of flexible manipulators, compliant structures, and active-based materials actuators/sensors.

Pedro Rodríguez-Ayerbe (M'10) was born in Zumarraga, Spain. He received the Technical Engineering diploma in electronics from Mondragon University, Mondragón, Spain, in 1993, and the Engineering degree in electrical engineering from the École Supérieure d'Électricité (Supélec), Gif-sur-Yvette, France, in 1996. He then received the Ph.D. degree in automatic control and the "Habilitation Diriger des Recherches" from Supélec and the Université Paris-Sud, Orsay, France, in 2002 and 2014, respectively.

Since 2004, he has been with the Automatic Control Department, CentraleSupélec, Gif-sur-Yvette, where he is currently an Associate Professor. From 1996 until 2000, he worked with Fagor Automation, Spain, and with Lore, France. His research interests include constrained predictive control and robust control theory.

Didier Dumur was born in Montreuil, France. He received the Engineering degree in electrical engineering from the Ecole Supérieure d'Électricité, Gif-sur-Yvette, France, in 1985. He then received the Ph.D. degree in automatic control and the "Habilitation Diriger des Recherches" from the Université Paris-Sud, Orsay, France, in 1993 and 2002, respectively.

Since 2003, he has been a Professor with the Automatic Control Department, CentraleSupélec, Gif-sur-Yvette, where he has been the Head of the Automatic Control Department since 2012. His current research interests include constrained and robust-predictive control for nonlinear and hybrid systems, with specific applications to robotics, bioreactors, thermal control of buildings, and complex systems such as energy networks.

Prof. Dumur is a Fellow of the International Academy for Production Engineering (CIRP).